




Antifungal Activity and Potential Action Mechanism of Allicin against *Trichosporon asahii*

 Xin Yang,^a Shuang Bai,^b Jiamin Wu,^b Yunlong Fan,^b Yuekun Zou,^b Zhikuan Xia,^b Junhong Ao,^b Tong Chen,^b Mingwang Zhang,^{b,c} Rongya Yang^{a,b}

^aDepartment of Dermatology, Yanbian University Hospital, Yanji, China

^bDepartment of Dermatology, The Seventh Medical Center of PLA General Hospital, Beijing, China

^cDepartment of Dermatology, Southwest Hospital, Army Medical University, Chongqing, China

ABSTRACT *Trichosporon asahii* is an emerging opportunistic pathogen that causes potentially fatal disseminated trichosporonosis. The global prevalence of coronavirus disease 2019 (COVID-19) poses an increasing fungal infection burden caused by *T. asahii*. Allicin is the main biologically active component with broad-spectrum antimicrobial activity in garlic. In this study, we performed an in-depth analysis of the antifungal characteristics of allicin against *T. asahii* based on physiological, cytological, and transcriptomic assessments. *In vitro*, allicin inhibited the growth of *T. asahii* planktonic cells and biofilm cells significantly. *In vivo*, allicin improved the mean survival time of mice with systemic trichosporonosis and reduced tissue fungal burden. Electron microscopy observations clearly demonstrated damage to *T. asahii* cell morphology and ultrastructure caused by allicin. Furthermore, allicin increased intracellular reactive oxygen species (ROS) accumulation, leading to oxidative stress damage in *T. asahii* cells. Transcriptome analysis showed that allicin treatment disturbed the biosynthesis of cell membrane and cell wall, glucose catabolism, and oxidative stress. The overexpression of multiple antioxidant enzymes and transporters may also place an additional burden on cells, causing them to collapse. Our findings shed new light on the potential of allicin as an alternative treatment strategy for trichosporonosis.

IMPORTANCE Systemic infection caused by *T. asahii* has recently been recognized as an important cause of mortality in hospitalized COVID-19 patients. Invasive trichosporonosis remains a significant challenge for clinicians, due to the limited therapeutic options. The present work suggests that allicin holds great potential as a therapeutic candidate for *T. asahii* infection. Allicin demonstrated potent *in vitro* antifungal activity and potential *in vivo* protective effects. In addition, transcriptome sequencing provided valuable insights into the antifungal effects of allicin.

KEYWORDS allicin, *Trichosporon asahii*, invasive trichosporonosis, COVID-19, biofilm, RNA-Seq, transcriptomics, oxidative stress

Invasive fungal infections represent a global problem resulting in millions of deaths every year. In recent years, with the evolving coronavirus disease 2019 (COVID-19) pandemic around the world, the incidence of invasive fungal infections has been drastically rising. Common invasive fungal infections of COVID-19 patients are caused by *Aspergillus* spp., *Candida* spp., and *Mucormycetes* (1). It is noteworthy that recent investigations discovered that hospitalized COVID-19 patients had a high risk of developing invasive trichosporonosis, a rare yeast infection mainly caused by *Trichosporon asahii* (2, 3). Systemic infection with this emergent yeast is most often fatal. According to statistics reported by Benelli et al., COVID-19 patients with invasive trichosporonosis had an 86% mortality rate (4).

Trichosporon spp. are basidiomycetous yeast-like fungal pathogens that are widely distributed in nature and found in parts of the human body, such as the skin, gastrointestinal

Editor Renato Kovacs, University of Debrecen

Copyright © 2023 Yang et al. This is an open-access article distributed under the terms of the [Creative Commons Attribution 4.0 International license](https://creativecommons.org/licenses/by/4.0/).

Address correspondence to Mingwang Zhang, mingwangzhang2@163.com, or Rongya Yang, yangrya@sina.com.

The authors declare no conflict of interest.

Received 3 March 2023

Accepted 26 April 2023

Published 18 May 2023

TABLE 1 MICs and MFCs of allicin and antifungals against *Trichosporon asahii*

| Strains | Allicin concn ($\mu\text{g ml}^{-1}$) at: | | | | | Fluconazole MIC ₅₀ ($\mu\text{g ml}^{-1}$) | Amphotericin B MIC ₁₀₀ ($\mu\text{g ml}^{-1}$) |
|-------------|---|-------------------|-------------------|-------------------|-----|--|--|
| | 24 h | | 48 h | | | | |
| | MIC ₅₀ | MIC ₉₀ | MIC ₅₀ | MIC ₉₀ | MFC | | |
| CBS 2479 | 8 | 32 | 64 | 128 | 256 | 2 | 2 |
| BMT 06-3-01 | 8 | 32 | 32 | 64 | 128 | 2 | 2 |
| BMT 06-3-02 | 16 | 32 | 32 | 64 | 128 | 2 | 2 |
| BMT 06-3-03 | 8 | 16 | 32 | 64 | 128 | 1 | 1 |
| BMT 06-3-04 | 8 | 16 | 128 | 256 | 256 | 2 | 2 |
| BMT 06-3-05 | 8 | 32 | 64 | 128 | 128 | 1 | 4 |
| BMT 06-3-06 | 8 | 32 | 64 | 128 | 128 | 2 | 4 |
| BMT 06-3-07 | 16 | 64 | 128 | 256 | 256 | 0.5 | 0.5 |
| BMT 06-3-08 | 8 | 64 | 64 | 128 | 256 | 2 | 2 |
| BMT 06-3-09 | 8 | 16 | 64 | 128 | 256 | 4 | 4 |
| BMT 06-3-10 | 16 | 32 | 64 | 128 | 256 | 1 | 2 |

tract, and respiratory tract. *T. asahii* is the predominant pathogen of *Trichosporon* spp., which is able to cause life-threatening invasive trichosporonosis, particularly in immunosuppressed patients (5). The management of patients with trichosporonosis remains a challenge, as few antifungal drugs are effective against the genus *Trichosporon*. *In vitro* studies suggest that *T. asahii* exhibits intrinsic resistance to echinocandins and poor susceptibility to amphotericin B. In contrast, the triazole antifungals, such as fluconazole and voriconazole, have better *in vitro* and *in vivo* antifungal activities against *T. asahii* and have been selected as preferred drugs for systematic trichosporonosis (6, 7). Unfortunately, the widespread use of the azoles has contributed to the rapid emergence of azoles-resistant *T. asahii* isolates and even multidrug-resistant isolates, posing serious challenges to the clinical treatment of trichosporonosis (8, 9). Thus, the development of innovative therapeutic strategies is imperative. At present, natural compounds or natural bioactive products have attracted much attention in treating infectious diseases due to their broad-spectrum antimicrobial activity and infrequent inducible drug resistance (10, 11).

Allicin (diallyl thiosulfinate) is an important organosulfur compound found in garlic and other *Allium* species, with a broad range of biological activities, such as antibacterial, antifungal, antiparasitic, and antiviral activities (12). Regarding the effects of allicin on fungi, numerous studies have demonstrated its remarkable antifungal activity against various clinically important fungal species, including *Candida* spp., *Cryptococcus* spp., *Aspergillus* spp., *Trichophyton* spp., and others (13). However, the antifungal activity and action mechanism of allicin against *Trichosporon* spp. have not been defined.

The current study sought to assess the antifungal property of allicin against *T. asahii* and investigate its underlying action mechanisms.

RESULTS

Antifungal susceptibility. Table 1 shows the *in vitro* susceptibility of *T. asahii* planktonic cells to allicin and antifungals. According to the tentative epidemiologic cutoff values (ECV_s) for fluconazole (FCZ) and amphotericin B (AmB) (14), all strains (11/11) were susceptible to FCZ and the majority of strains (9/11) were resistant to AmB. The MICs of allicin against *T. asahii* varied significantly between 24 h and 48 h of incubation. The MIC₅₀ and MIC₉₀ ranges were 8 to 16 $\mu\text{g mL}^{-1}$ and 16 to 64 $\mu\text{g mL}^{-1}$ at 24 h and were 32 to 128 $\mu\text{g mL}^{-1}$ and 64 to 256 $\mu\text{g mL}^{-1}$ at 48 h. Allicin was highly active against all *T. asahii* strains, with the three clinical isolates exhibiting the greatest sensitivity (MIC₉₀ of 64 $\mu\text{g mL}^{-1}$) at the 24-h reading. The minimum fungicidal concentrations (MFCs) of allicin against *T. asahii* ranged from 128 $\mu\text{g mL}^{-1}$ to 256 $\mu\text{g mL}^{-1}$, with an average of 197.81 $\mu\text{g mL}^{-1}$.

Spot assays. Spot assays showed the efficacy of allicin against *T. asahii* strains in a visual form (Fig. 1A and B). Significant growth reduction was observed as the allicin concentration increased. The results showed an excellent correlation with the microdilution broth assay.

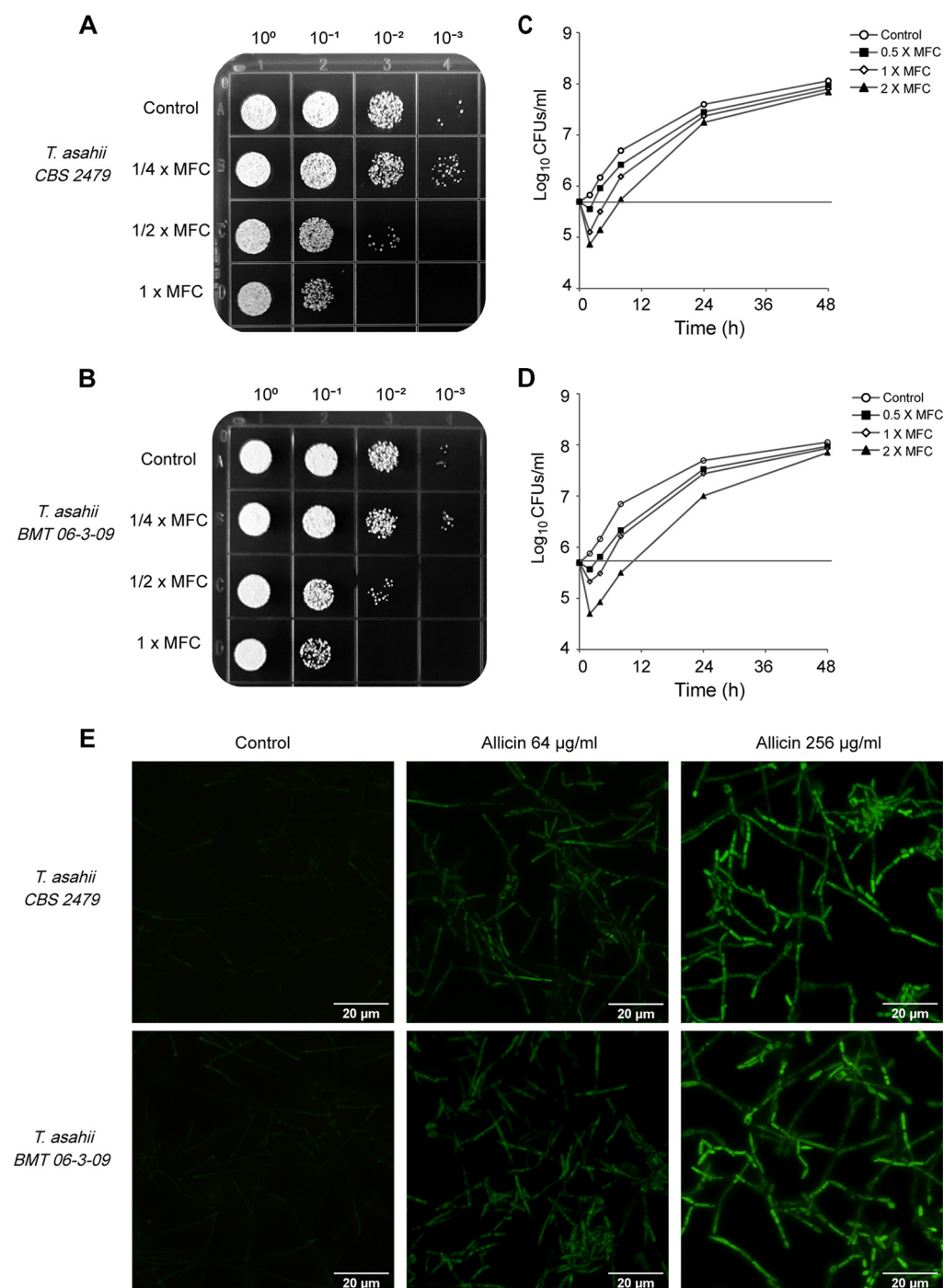


FIG 1 Spot assays (A and B) and time-kill curves (C and D) validated the inhibitory effect of allicin on *T. asahii* growth *in vitro*. (E) The intracellular ROS changes in *T. asahii* cells exposed to allicin were detected using the fluorescent probe DCFH-DA. Magnification, $\times 200$.

Time-kill studies. To further confirm the antifungal activity of allicin, a time-kill curve assay was carried out. As shown in Fig. 1C and D, allicin at 2 \times MFC showed distinct fungicidal activity during the first 8 h of incubation, with maximum reductions in viable counts reaching 1.02 log₁₀ CFU mL⁻¹ at 4 h for *T. asahii* CBS 2479 and 1.34 log₁₀ CFU mL⁻¹ at 8 h for *T. asahii* BMT 06-3-09. However, the full fungicidal end points (99.9% killing) could not be achieved with allicin throughout the incubation period of up to 48 h.

Antibiofilm activity. The results of the XTT [2,3-bis-(2-methoxy-4-nitro-5-sulfo-phenyl)-2H-tetrazolium-5-carboxanilide salt] reduction assay are shown in Fig. 2. Allicin

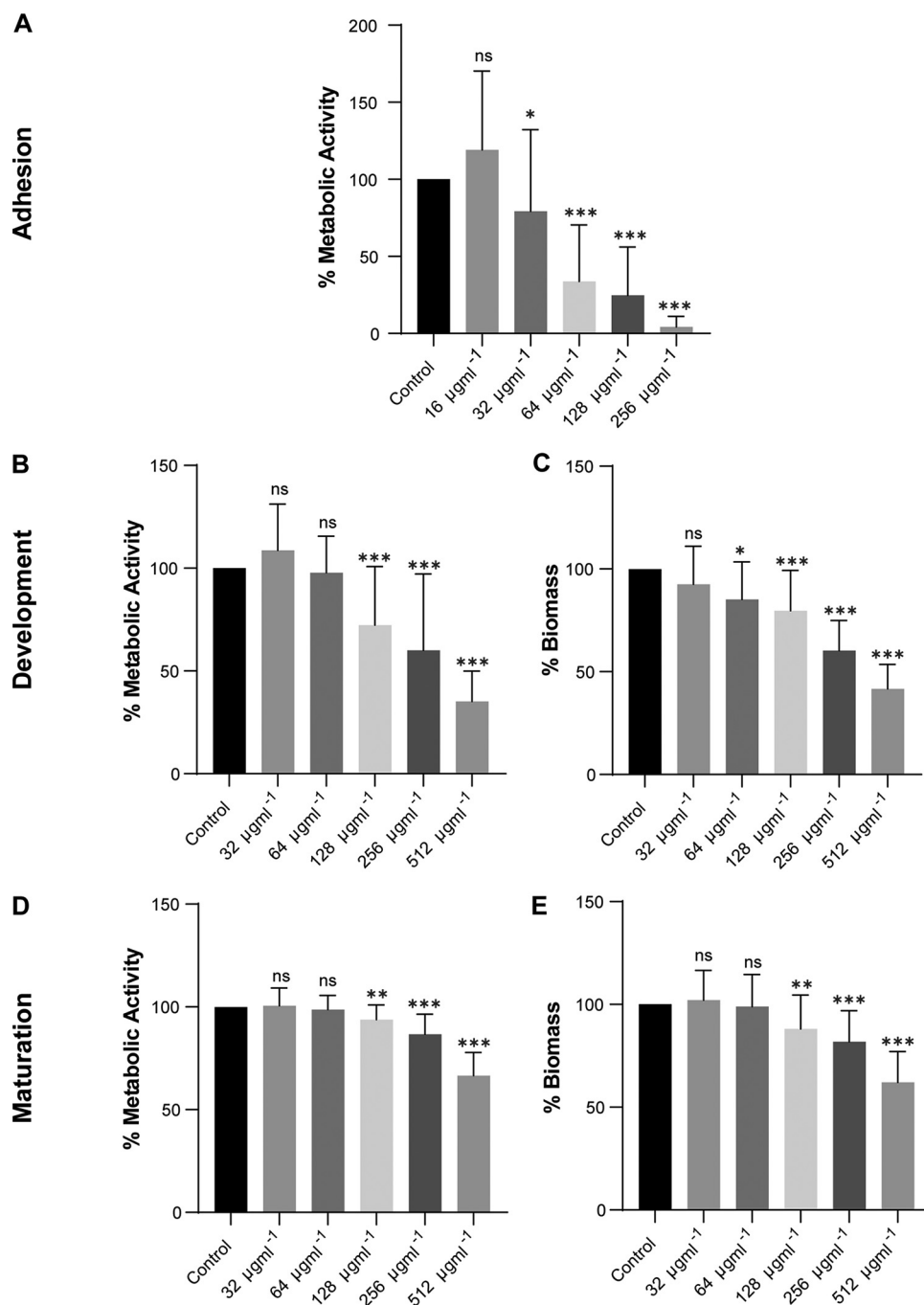


FIG 2 Effect of allicin on the metabolic activity and biomass of *T. asahii* ($n = 6$) biofilms in different growth stages, expressed as relative percentages of the absorbance of the XTT reduction assay (A, B, and D) and crystal violet staining (C and E), respectively. Adhesion of *T. asahii* cells after incubation for 6 h (A), after growth for 24 h (B and C), and in 48-h mature biofilms (D and E). ns, not significant; *, $P < 0.05$; **, $P < 0.01$; ***, $P < 0.001$ versus the control.

inhibited the metabolic activity of *T. asahii* biofilms in a dose-dependent manner. Compared to the control, $32 \mu\text{g mL}^{-1}$ allicin inhibited biofilm adhesion by 20.8%, whereas $256 \mu\text{g mL}^{-1}$ allicin inhibited biofilm adhesion almost completely (Fig. 2A). However, with the development and maturity of biofilms, increased resistance to allicin was observed in *T. asahii* biofilm cells. Compared to the control, $256 \mu\text{g mL}^{-1}$ allicin inhibited biofilm activity by approximately 40.0% in the development stage and 13.3% in the maturation stage (Fig. 2B and D). The results of the crystal violet (CV) assay showed that in the presence of allicin, the biomass production of *T. asahii* biofilms was significantly reduced (Fig. 2C).

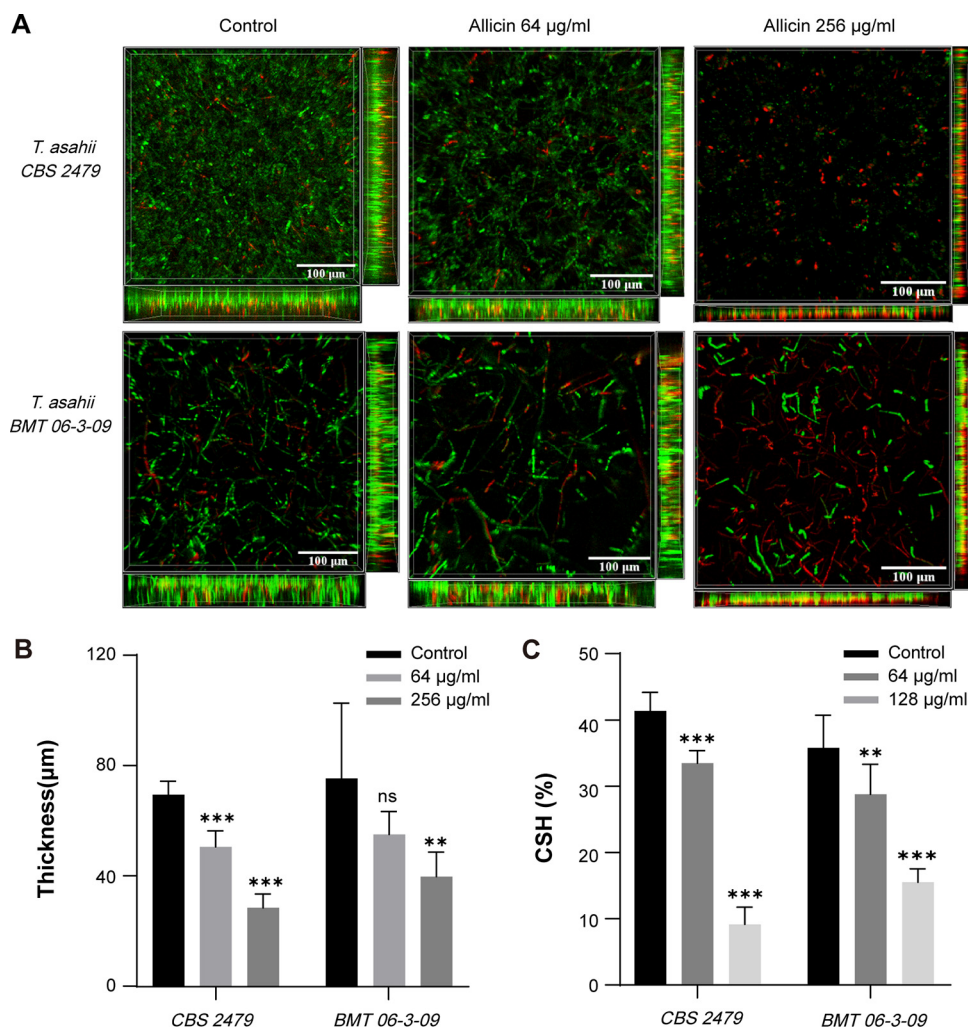


FIG 3 (A) CLSM images of *T. asahii* biofilms following treatment with allicin. SYTO 9 shows live cells (green), and PI shows dead or damaged cells (red). Magnification, $\times 400$. (B) Quantitative analysis of biofilm thickness in CLSM images. (C) Effect of allicin on cell surface hydrophobicity of *T. asahii* ($n = 3$).

Likewise, even at high concentrations, allicin exhibited limited activity against mature *T. asahii* biofilms. Allicin at $256 \mu\text{g mL}^{-1}$ caused a reduction in biomass of just 18.9% in mature biofilms compared with the untreated control (Fig. 2E).

Figure 3A shows confocal laser scanning microscopy (CLSM) images of *T. asahii* biofilms, where live cells were stained green by SYTO 9 and dead/damaged cells were stained red by propidium iodide (PI). Control samples presented compact and dense biofilms. In contrast, allicin treatment resulted in a scattered biofilm structure dominated by dead cells (red) and significantly reduced biofilm thickness (Fig. 3B). The decrease in biomass was concomitant with a decline in biofilm cell viability, which corroborates the results of the XTT and CV assays.

CSH. The changes in cell surface hydrophobicity (CSH) of planktonic *T. asahii* cells were evaluated following exposure to allicin using a water-hydrocarbon two-phase assay. The results showed that allicin significantly decreased the cell surface hydrophobicity of *T. asahii*, with an 83.76% reduction observed at $128 \mu\text{g mL}^{-1}$ compared to the control group (Fig. 3C).

ROS accumulation. Intracellular levels of reactive oxygen species (ROS) in *T. asahii* were assessed by the dichlorodihydrofluorescein diacetate (DCFH-DA) assay (Fig. 1E). The *T. asahii* cells treated with allicin exhibited strong green fluorescence, whereas only weak fluorescence was observed in untreated cells. This suggests that allicin is able to increase accumulation of intracellular ROS.

TABLE 2 MICs of allicin against *Trichosporon asahii* in the presence and absence of ergosterol at the 48-h reading^a

| Strain | MIC ₅₀ ($\mu\text{g ml}^{-1}$) of allicin | | MIC ₉₀ ($\mu\text{g ml}^{-1}$) of allicin | | MIC ₁₀₀ ($\mu\text{g ml}^{-1}$) of AmB | |
|-------------|--|-----------------|--|-----------------|---|-----------------|
| | Without ergosterol | With ergosterol | Without ergosterol | With ergosterol | Without ergosterol | With ergosterol |
| CBS 2479 | 64 | >256 | 128 | >256 | 2 | 8 |
| BMT 06-3-01 | 32 | 128 | 64 | >256 | 2 | 4 |
| BMT 06-3-02 | 32 | 64 | 64 | 128 | 2 | 2 |
| BMT 06-3-03 | 32 | 64 | 64 | 256 | 1 | 1 |
| BMT 06-3-04 | 128 | >256 | 256 | >256 | 2 | 4 |
| BMT 06-3-05 | 64 | 256 | 128 | >256 | 4 | 4 |
| BMT 06-3-06 | 64 | >256 | 128 | >256 | 4 | 8 |
| BMT 06-3-07 | 128 | >256 | 256 | >256 | 0.5 | 2 |
| BMT 06-3-08 | 64 | 256 | 128 | >256 | 2 | 4 |
| BMT 06-3-09 | 64 | >256 | 128 | >256 | 4 | 8 |
| BMT 06-3-10 | 64 | >256 | 128 | >256 | 2 | 4 |

^aErgosterol was used at 200 $\mu\text{g ml}^{-1}$.

Ergosterol assay. The effect of allicin on the *T. asahii* cell membrane was evaluated using the ergosterol assay. AmB was set as the positive control for ergosterol assay due to its antifungal action depending on interaction with fungal cell membrane ergosterol. The activities of allicin and AmB against *T. asahii* were significantly suppressed in the presence of ergosterol. For a large proportion of *T. asahii* strains (9/11), the MICs of AmB increased 2-fold or 4-fold in the presence of ergosterol. Similarly, an obvious increase in MICs of allicin was also observed for all *T. asahii* strains (11/11) in the presence of ergosterol (Table 2). The findings indicate that the antifungal activity of allicin is related to its effect on cell membrane ergosterol of *T. asahii*.

Sorbitol assay. In addition, the effect of allicin on the cell wall of *T. asahii* was evaluated with a sorbitol assay. When fungi are exposed to drugs that act on the cell wall, sorbitol is capable of maintaining proper osmotic pressure. AmB was set as the negative control in sorbitol assay. The antifungal activity of AmB is unlikely affected by sorbitol, in view of its mode of action (15). Unexpectedly, the MICs of AmB increased significantly in the presence of sorbitol compared to the control (data not shown). A likely explanation is that the sorbitol reduces total ergosterol of *T. asahii* cells (16). As a result, evidence of the effect of allicin on the *T. asahii* cell wall was not able to be obtained by the sorbitol assay.

Morphology and ultrastructure. The effect of allicin on the morphology of *T. asahii* was observed using scanning electron microscopy (SEM) (Fig. 4A to F). The untreated cells possessed normal shapes and smooth surfaces, while allicin-treated *T. asahii* cells exhibited rough pitted surfaces and a severely shriveled appearance.

The ultrastructure changes of *T. asahii* cells were examined using transmission electron microscopy (TEM) (Fig. 4G to L). Untreated cells exhibited complete cell walls, plasma membranes, and organelles. In contrast, allicin caused significant cellular damage, including structural disturbances with nonuniform thickness, irregular plasma membranes and obvious vacuolation.

Anti-*T. asahii* activity in vivo. The *in vivo* protective effect of allicin was evaluated in the murine model with systemic trichosporonosis. Experimental mice were treated with allicin or saline for 7 consecutive days. The final results showed that the mean survival time (MST) was 6.5 days in saline-treated mice; in contrast, treatment with 20 mg kg⁻¹ allicin prolonged MST of mice to 9.4 days ($P < 0.01$). However, there were no significant differences in MST of mice between the group receiving 10 mg kg⁻¹ allicin (MST of 6.9 days) and the saline group ($P > 0.05$). By the end of the trial, one mouse was still alive in the group receiving 20 mg kg⁻¹ allicin, whereas all mice in the other two groups died (Fig. 5A).

The severity of *T. asahii* infection was assessed by determining the tissue fungal burden of mice from various experimental groups. Quantification of fungal burden in the control group revealed that the spleen ($7.43 \pm 0.11 \log_{10}$ CFU/g) was the most severely involved tissue, followed closely by liver ($6.29 \pm 0.07 \log_{10}$ CFU/g) and kidney ($5.43 \pm 0.09 \log_{10}$ CFU/g). Compared to the control, a significant reduction in tissue fungal burden was observed in the group receiving 20 mg kg⁻¹ allicin (47.19%

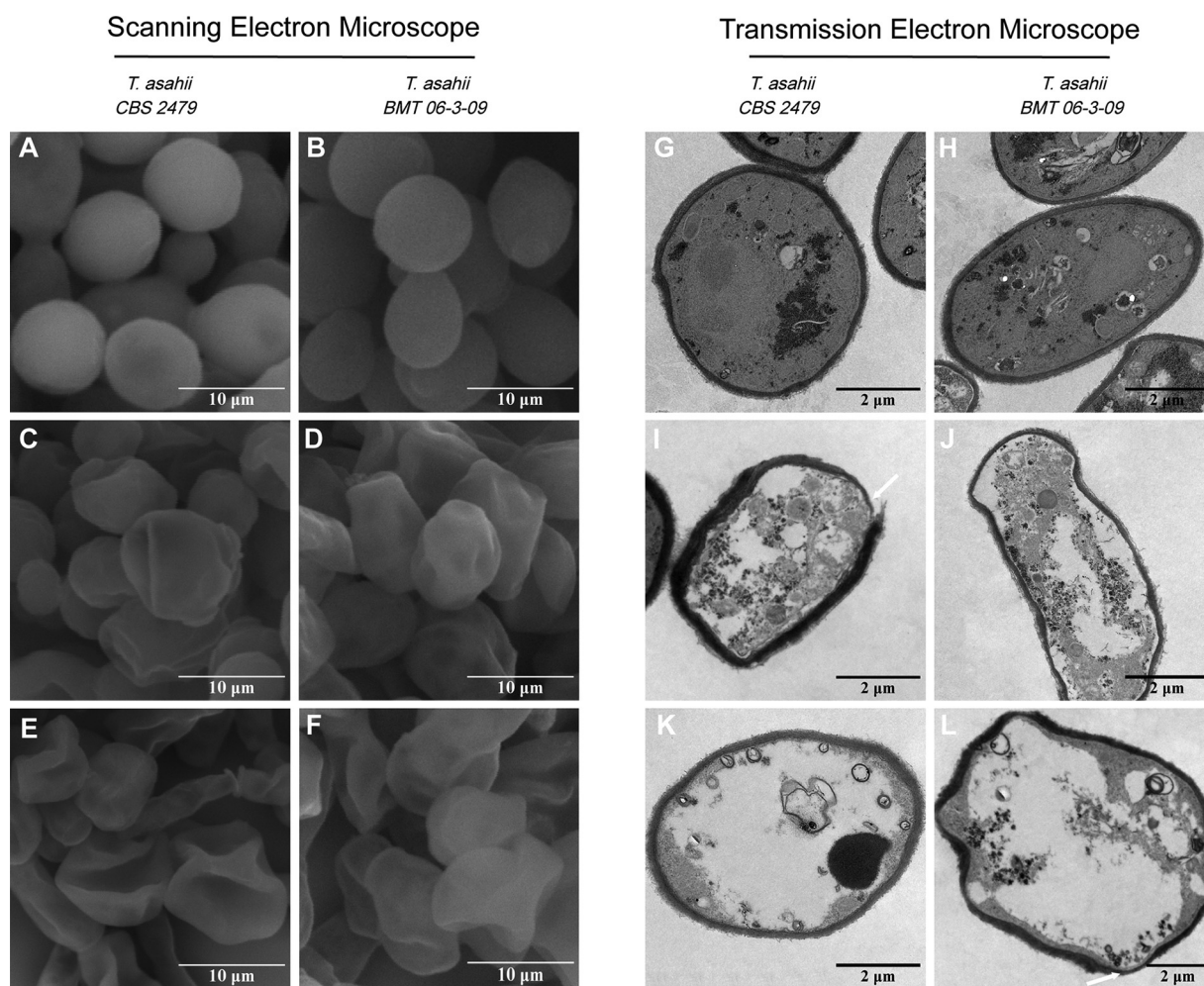


FIG 4 SEM and TEM images of *T. asahii* cells. (A, B, G, and H) Control cells. (C to F) The allicin-treated cells became irregular, pitted, and shriveled in SEM images. Notable structural disorganization within the cytoplasm (I and J), obvious vacuolation (K and L), nonuniform thickness, irregular plasma membrane, and degraded cell wall (white arrows) were observed in allicin-treated cells by TEM. Magnifications, $\times 7,000$ for SEM and $\times 3,000$ for TEM.

reduction in kidney [$P < 0.01$]; 45.42% reduction in liver [$P < 0.001$]; 35.83% reduction in spleen [$P < 0.05$] (Fig. 5B and C).

Transcriptome sequencing (RNA-Seq) quality and mapping rate. A total of 245,150,678 raw reads with adapters and low-quality reads were identified. Following quality control, 1,403,742 reads were filtered out, leaving 243,746,936 high-quality clean reads for further analysis. The rRNA mapped reads were removed before read alignment, and approximately 89.22% of the paired-end clean reads were mapped to the reference genome, containing approximately 88.34% uniquely mapped reads. Table 3 summarizes the information presented above.

DEG analysis. In this study, the transcriptome expression profiles of *T. asahii* were significantly affected under allicin stress. A total of 1,595 genes were identified as differentially expressed genes (DEGs) according with the filter criteria (absolute value of fold change $|\text{FC}| \geq 1.5$; false discovery rate $[\text{FDR}] < 0.05$). Among these DEGs, 873 were upregulated and 722 were downregulated in the allicin-exposed samples compared to the untreated samples. The difference in quantity between upregulated and downregulated genes was less than 10% of total DEGs. Hierarchical cluster analysis of DEGs revealed intragroup coherence and intergroup difference, indicating that the data were highly reliable (Fig. 6A and B; also, see Table S1 in the supplemental material).

Functional enrichment analysis. To obtain further insight into biological responses of *T. asahii* to allicin, a functional enrichment analysis, including GO (Gene Ontology)

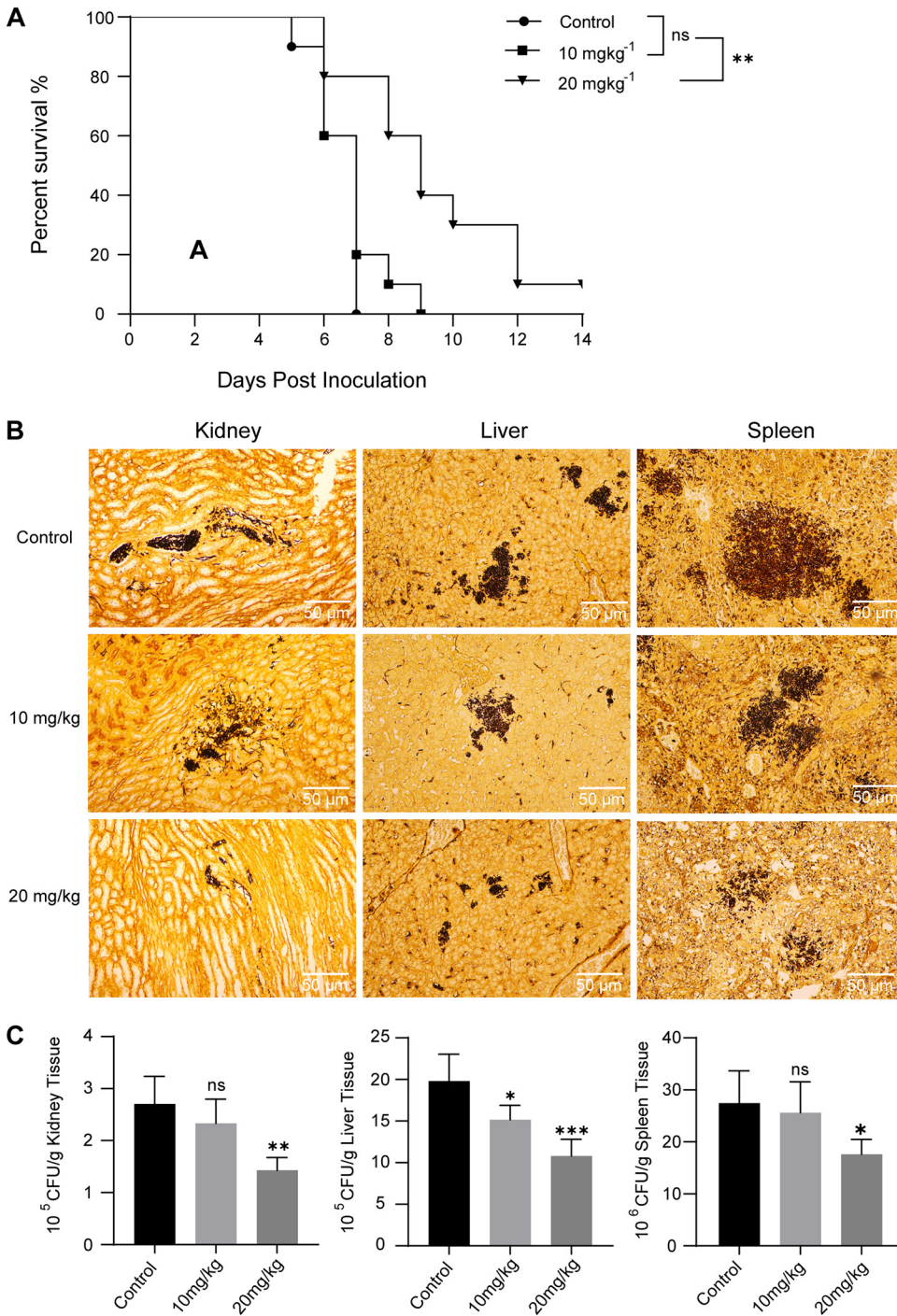


FIG 5 (A) Survival curves in mice inoculated intravenously with *T. asahii* BMT 06-3-09 and treated with physiological saline (i.p.) or allicin (i.p.). Treatment started 3 days before *T. asahii*-induced infections and lasted until 4 days postinfection. Mice were monitored until day 14 postinfection. Each group consisted of 10 mice for survival analysis. (B) Tissue fungal burden of mice was visualized using GMS stain at 5 days postinfection. Fungal cells were stained black by GMS. Magnification: $\times 200$. (C) Quantitative analysis of tissue fungal burden, expressed as CFU per gram. ns, not significant; *, $P < 0.05$; **, $P < 0.01$; ***, $P < 0.001$ versus control.

functional categories and KEGG (Kyoto Encyclopedia Genes and Genomes) pathways, was performed on the up- and downregulated genes.

A total of 1,045 DEGs (65.5% of total) were mapped to three GO categories with 116 GO terms, including 15 cellular component terms (GO: CC), 54 molecular function terms (GO: MF), and 47 biological processes terms (GO: BP). In the cellular component category, "plasma membrane" and "mitochondrion" were the principal enriched components. In the

TABLE 3 RNA-Seq quality and mapping rate

| Sample | No. of reads | | No. (%) mapped | |
|-------------|--------------|------------|--------------------|--------------------|
| | Raw | Clean | Unique | Total |
| Treatment-1 | 37,422,164 | 37,208,550 | 31,966,951 (88.31) | 32,318,614 (89.28) |
| Treatment-2 | 40,934,342 | 40,685,208 | 35,090,109 (88.02) | 35,454,883 (88.93) |
| Treatment-3 | 40,951,936 | 40,725,356 | 34,569,483 (88.41) | 34,935,426 (89.35) |
| Control-1 | 41,914,734 | 41,659,424 | 36,443,554 (88.06) | 36,753,254 (88.81) |
| Control-2 | 44,627,768 | 44,364,542 | 38,772,765 (88.24) | 39,138,560 (89.07) |
| Control-3 | 39,299,734 | 39,103,856 | 34,611,277 (89.03) | 34,930,701 (89.86) |

molecular function category, “catalytic activity (GO:0003824),” “oxidoreductase activity (GO:0016491),” “cofactor binding (GO:0048037),” and “transporter activity (GO:0005215)” were important enriched terms. Terms of small-molecule metabolic and biosynthetic process were significantly enriched in the biological processes category, including “organic acid metabolic process (GO:0006082),” “drug metabolic process (GO:0017144),” “cellular amino acid biosynthetic process (GO:0008652),” and so on (Fig. 7A to C; Table S2).

In KEGG enrichment analysis, 303 DEGs (19.0% of total) were mapped to 5 KEGG categories with 107 pathways, including 1 organismal system term, 3 environmental information processing terms, 8 cellular process terms, 19 genetic information processing terms, and 76 metabolism terms, without considering significance levels. Some pathways associated with signal transduction (such as MAPK signaling pathway [ko04011] and phosphatidylinositol signaling system [ko04070]), energy metabolism (such as oxidative phosphorylation [ko00190]), amino acid metabolism (such as tryptophan metabolism [ko00380], cysteine and methionine metabolism [ko00270], and glycine, serine, and threonine metabolism [ko00260]), lipid metabolism (such as steroid biosynthesis [ko00100] and biosynthesis of unsaturated fatty acids [ko01040]), membrane transport (such as ABC transporters [ko02010]), and gene replication, transcription, and translation (such as DNA replication [ko03030], nucleotide excision repair [ko03420], RNA polymerase [ko03020], and ribosome [ko03010]) were impacted by treatment with allicin (Fig. 7D; Table S3).

In general, the functional enrichment analysis showed that large numbers of complex cellular elements and pathways are involved in the response of *T. asahii* to allicin stress.

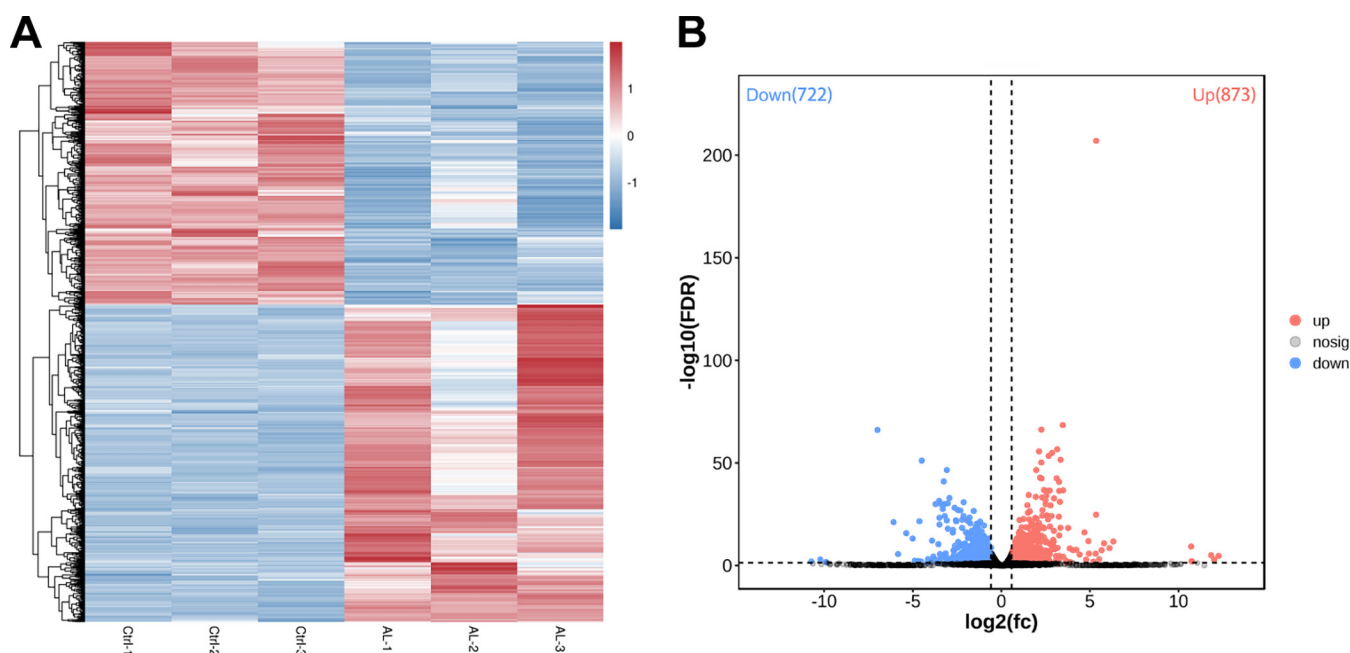


FIG 6 Transcriptome differences induced by allicin in *T. asahii* CBS 2479. (A) Heat map of DEGs. Hierarchical clustering analysis of DEGs according to the color scale indicates gene expression changes. (B) Volcano plot of DEGs. Red represents upregulated DEGs, and blue represents downregulated DEGs.

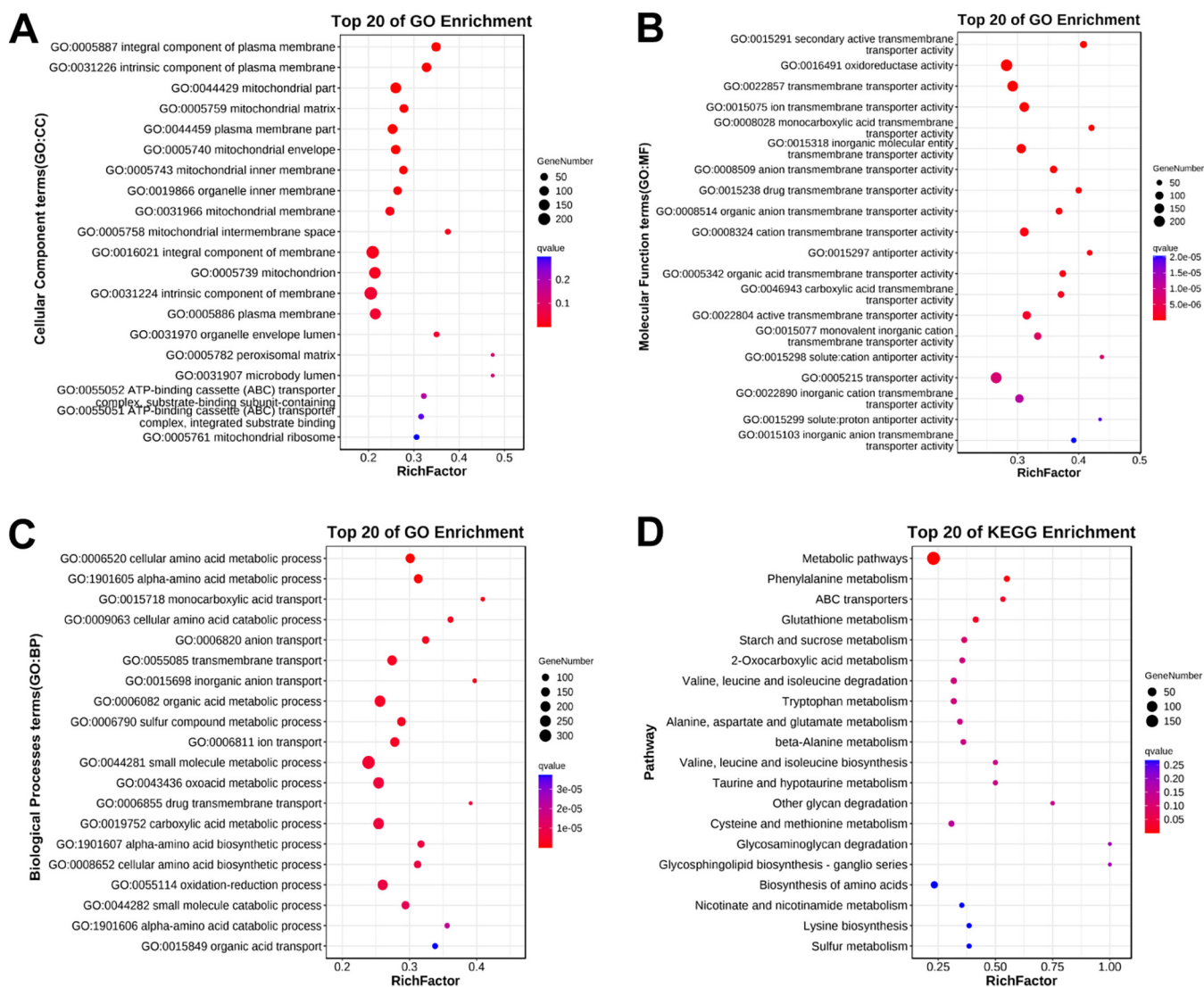


FIG 7 GO enrichment analysis and KEGG pathway analysis. (A) Top 20 cellular component terms in GO categories. (B) Top 20 molecular function terms in GO categories. (C) Top 20 biological processes terms in GO categories. (D) Top 20 KEGG pathways.

PHI-base analysis. PHI-base (Pathogen-Host Interactions Database) is a multispecies phenotype database devoted to exploration of pathogen-host interactions. In this study, the 335 DEGs (21% of total) were mapped to 6 phenotype categories: reduced virulence (55.22%, 185/335), unaffected pathogenicity (27.46%, 92/335), loss of pathogenicity (12.84%, 43/335), lethality (2.99%, 10/335), increased virulence (hypervirulence) (1.19%, 4/335), and chemistry target: resistance to chemical (0.30%, 1/335) (Table S6).

Validation of RNA-Seq through qRT-PCR analysis. To validate the expression levels of the DEGs identified in the transcriptomic analysis, five genes were selected to confirm their expression using quantitative reverse transcription-PCR (qRT-PCR). As shown in Fig. 8, the congruent expression trends observed between qRT-PCR and RNA-Seq analysis serve to validate the reliability of our transcriptome data.

DISCUSSION

Currently, only a few antifungal agents are approved for the treatment of invasive fungal infections: azoles, polyenes, and echinocandins (17). The emergence of resistant strains complicates patient management. Thus, there is a pressing need for novel antifungal agents. Medicinal plants have been proven to be an invaluable resource for exploring pharmacologically active molecules. In recent years, a large number of medicinal plants or

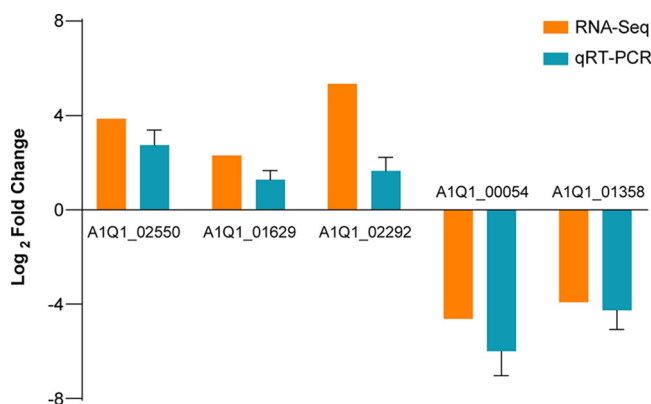


FIG 8 qRT-PCR analysis to validate the genes in RNA-Seq data. Relative expression level of DEGs is shown using an index of \log_2 fold change.

their derivatives have undergone examination for their pharmacological activities. Garlic (*Allium sativum* L.) is an aromatic herbaceous plant whose extracts and isolated compounds possess various biological activities, including anticarcinogenic, antiparasitic, antibacterial, and antifungal activities. Allicin is the most biologically active sulfur-containing compound in garlic (18, 19). The purpose of this study was to investigate the activities and mechanisms of allicin against *T. asahii*.

In this study, *in vitro* susceptibility testing demonstrated that allicin was highly active against *T. asahii*. Although allicin has been reported to exhibit significant inhibitory activity against various microorganisms, MICs of allicin vary slightly among different species (20–22). In addition to species differences, the discrepancies in MICs for allicin may be also attributed to differences in drug sources and antifungal susceptibility testing assays. Moreover, the effectiveness of allicin against *T. asahii* was further confirmed by a spot assay and a time-kill study. It is noteworthy that all tested concentrations of allicin were unable to reach the full fungicidal endpoints (99.9% killing). This demonstrates that allicin lacks potent fungicidal effect on *T. asahii*. Another observation was the inhibitory effect of allicin on *T. asahii* biofilms. The formation of biofilms plays an important role in the pathogenesis of *Trichosporon* catheter-related bloodstream infections and poses significant challenges for treatment and eradication, often leading to persistent or recurrent infections despite treatment with antifungals (7, 23). In this research, allicin significantly inhibited the growth of nascent *T. asahii* biofilms while only weakly inhibiting mature biofilms. The antibiofilm activity of allicin has been demonstrated in multiple microorganisms, such as *Candida albicans*, *Staphylococcus aureus*, *Escherichia coli*, and *Proteus mirabilis* (24–26). Researchers also found that allicin could exert antibiofilm effects by downregulating the expression of key genes related to biofilm formation. For example, Khodavandi et al. (27) reported that allicin significantly decreased the gene expression of HWP1, which has been proved to be essential for *Candida albicans* biofilm adherence (28). However, in the current study, we were unable to verify the expression of biofilm-related genes as other researchers have done, as no studies have been performed to identify specific genes or biological pathways related to *T. asahii* biofilms. Therefore, the intricate molecular mechanism underlying allicin-mediated antibiofilm activity remains to be further studied.

Surface adhesion is regarded as an important first step in the biofilm formation. The intrinsic high-level cell surface hydrophobicity of *T. asahii* cells is responsible for their rapid surface adhesion (29, 30). To explore the effect of allicin on *T. asahii* surface adhesion, a CSH assay was performed in this study. The results showed that allicin treatment remarkably reduced surface hydrophobicity of *T. asahii* cells, thus interfering with the cell-substratum interaction, which provided a possible explanation for the inhibitory effects of allicin on *T. asahii* biofilm adhesion.

In vivo antifungal activity of allicin has also been demonstrated in previous studies. In this study, allicin was administered intravenously to mice 3 days before *T. asahii*-

induced infections and treatment lasted until 4 days postinfection. The survival analysis results showed that the MST of saline-treated mice was 6.5 days postinfection, whereas the MST of mice receiving 20 mg kg⁻¹ allicin was 9.4 days ($P < 0.01$). Meanwhile, 20 mg kg⁻¹ allicin significantly reduced the fungal burden in kidney ($P < 0.01$), spleen ($P < 0.05$), and liver ($P < 0.001$), compared to the control. These findings suggest a superior protective effect of allicin *in vivo*. Furthermore, our previous investigation demonstrated the absence of mortality and significant visceral damage in uninfected mice subjected to 20 mg kg⁻¹ allicin treatment for 1 week, thus highlighting the safety profile of allicin at this dosage (Fig. S1). Koch et al. reported that intravenous injection of allicin at 60 mg kg⁻¹ is lethal for mice (31). As we know, the survival rate of mice can be affected by several major factors, such as *T. asahii* virulence, efficacy of immunosuppression, and dosages of allicin. Based on the evidence presented above, further research is required to investigate whether higher dosages of allicin can further prolong survival of mice with systemic trichosporonosis, assuming that it is safe and nontoxic.

In our study, GO enrichment analysis showed that the plasma membrane was one of the most enriched components, implying that composition and integrity of the plasma membrane of *T. asahii* are greatly affected by allicin. Further analysis found that several genes encoding essential enzymes in the ergosterol biosynthesis pathway (Table S4), such as C-4 methyl sterol oxidase (ERG25), sterol 24-C-methyltransferase (ERG6), and lanosterol 14- α -demethylase (ERG11), were downregulated, indicating that allicin caused a reduction in ergosterol content. Ergosterol, an important component of fungal plasma membranes, plays an essential role in maintaining a variety of cellular functions, including membrane integrity, membrane fluidity, and membrane-associated proteins activity, and has always been an important target for antifungal-drug development. On the other hand, the ergosterol assay suggested that allicin may interact with plasma membrane ergosterol. In addition, oxidative stress induced by allicin was capable of disrupting plasma membrane via phospholipid peroxidation (20). Previous cytological researches confirmed the effects of allicin on fungal plasma membrane. Ogita et al. found that in *Saccharomyces cerevisiae*, allicin enhanced fungicidal activity of AmB by inhibiting ergosterol trafficking from the plasma membrane to the vacuole membrane (32). Li et al. recently reported that allicin exerted antifungal efficacy against *Cryptococcus neoformans* by regulating plasma membrane-related pathways to block the cell membrane (33). The effects of allicin on fungal cell membrane were also reported by Khodavandi et al., Aala et al., and Kim et al. (27, 34, 35).

The cell wall is indispensable for maintaining fungal cellular homeostasis, as it serves to safeguard the cell against osmotic stress and mechanical injury while also contributing to the establishment of cellular morphology. In fact, the cell wall has been an important antimicrobial target due to its absence in human cells. In a recent study, researchers determined the effect of allicin on *Staphylococcus aureus* cell wall by matrix-assisted laser desorption ionization–time-of-flight (MALDI-TOF) mass spectrometry and identified Fem enzymes as a potential target for allicin in peptidoglycan synthesis (36). In addition, a study on *Aspergillus* spp. indicated that allicin could selectively target cell wall biosynthesis, thereby disrupting the structural integrity of the cell wall (37, 38). In present study, allicin was found to inhibit the expression of genes encoding 1,3- β -glucan synthase and chitin synthase (Table S4), which are mainly responsible for regulating biosynthesis of glucan and chitin, two essential components of the fungal cell wall. In addition, genes encoding glycosylphosphatidylinositol (GPI)-anchored protein were also observed to be downregulated (Table S4). The GPI-anchored proteins participate in a variety of cellular processes in fungal pathogens (39, 40). Most notably, they mediate posttranslational modification related to plasma membrane and cell wall organization, leading to the transportation of diverse proteins from the endoplasmic reticulum to the cell wall and ensuring the integrity of the cell wall. Antifungals targeting the GPI anchor synthesis pathway have been developed and have shown remarkable fungistatic activity in mice with disseminated fungal infection (41). We speculate

that allicin-induced damage to plasma membranes and cell walls may increase cell permeability, leading to an osmotic imbalance and ultimately resulting in cell inflation and collapse. SEM and TEM observations further confirmed degradation and disturbance of *T. asahii* cell structures caused by allicin.

The mitochondrion is another principal enriched component after exposure to allicin. Mitochondria are the major energy production centers in eukaryotes. Further analysis revealed that the majority of genes related to the mitochondrial respiratory chain and oxidative phosphorylation were upregulated (Table S4). Among them, cytochrome *c* oxidase and NADH-ubiquinone oxidoreductase participate in the formation of the respiratory chain complex, which serves as a crucial site for ATP production by coupling oxidation with phosphorylation in mitochondria (42). This implies an immediate requirement for energy to repair cellular damage and sustain regular cellular activity in response to allicin exposure of *T. asahii*. However, the genes encoding pyruvate dehydrogenase (Table S4), such as pyruvate dehydrogenase (E1) and dihydrolipoyl transacetylase (E2), were downregulated following allicin treatment. The pyruvate dehydrogenase complex catalyzes oxidation decarboxylation of pyruvate to produce acetyl coenzyme A (acetyl-CoA), which is a key step in aerobic oxidation of glucose and serves as a critical link between glycolysis and the tricarboxylic acid cycle (43). Thus, it is postulated that inhibition of glucose catabolism may be one of the potential antifungal mechanisms of allicin, leading to energy deficiency and ultimately accelerating cell death. The mitochondrial respiratory chain is the main source of ROS. In the process of electron transfer, leaked electrons are picked up by oxygen to produce ROS (44). DCFH-DA analysis showed that allicin-treated *T. asahii* cells exhibited a high level of intracellular ROS accumulation. ROS play an important role in the regulation of cell survival. The moderate levels of ROS promote cell proliferation and survival. In contrast, excessive ROS induce oxidative stress, leading to oxygenation damage, such as DNA strand breakage, protein degeneration, phospholipid peroxidation, and even cell death (45, 46). Among these, plasma membrane phospholipids are regarded as a target of oxidative stress, which helps to partly explain the plasma membrane damage caused by allicin. To respond to oxidative stress induced by allicin, antioxidant systems were activated in *T. asahii* cells, resulting in upregulation of genes encoding catalase (CAT), glutathione peroxidase (GPx), glutathione reductase (GR), peroxidase (PO), and superoxide dismutase (SOD) (Table S4). These antioxidant enzymes together constitute the cellular defense system to mitigate intracellular ROS accumulation and maintain redox homeostasis (47).

Another important finding is that allicin increased the expression of ATP-binding cassette (ABC) transporter-related genes (Table S4), such as the YOR1, Pdr11, and MDR1 genes. The ABC transporters are present in cellular and intracellular membranes and are involved in the import and removal of substances from cells and tissues, including drug transmembrane transport (48). This suggests that drug efflux systems mediated by ABC transporters were activated in *T. asahii* cells to decrease intracellular allicin concentrations and protect cells from allicin stress.

KEGG analysis showed a general upregulation of genes involved in replication, repair, transcription, and translation pathways (Table S5). As a compensatory mechanism, protein synthesis is strengthened, resulting in increased protein production to maintain normal cell activities and repair cell damage caused by allicin stress. Nevertheless, with mitochondrial dysfunction, the enhancement of cell damage repair and drug efflux may place an additional burden on *T. asahii* cells, accelerating cells collapse.

Aside from GO and KEGG analysis, we discovered that a small portion of DEGs were annotated in PHI-base (Table S6), implying potential effects of allicin on the pathogenicity and virulence of *T. asahii*. However, these details remain unclear and require extensive investigation (49).

We aware that our research has some limitations. First, specific targets of allicin have yet to be verified, and this will be the focus of our follow-up research. Second, researchers proposed that allicin may function better in combination with antifungal

drugs than when used alone (50). Thus, more studies need to be carried out to determine the *in vivo* and *in vitro* antifungal activities of allicin in combination with azoles against *T. asahii* in future work.

In conclusion, allicin treatment effectively inhibited *T. asahii* planktonic cells growth, interfered with biofilm formation, and exhibited positively protective effects in mice with systemic trichosporonosis, indicating the high potential of allicin as a potent antifungal candidate for treatment of *T. asahii* infection. Electron microscopy and biochemical analysis showed that cellular morphology and ultrastructure were damaged and ROS overproduction was induced following exposure to allicin, suppressing the growth of *T. asahii*. In addition, based on RNA-Seq analysis, the changes in transcriptome profiling of *T. asahii* following exposure to allicin were first revealed in our study, investigating underlying action mechanisms of allicin at the molecular level.

MATERIALS AND METHODS

Strains. In this study, a total of 11 *T. asahii* strains were used, including the type strain CBS 2479 and 10 common clinical isolates. All isolates were identified based on sequencing of the IGS1 region (51). The strains were routinely stored at -80°C . Before the start of an experiment, strains were plated on potato dextrose agar (PDA) medium to sustain optimal vitality through passage cultivation at 35°C .

Determination of MICs. The microdilution broth method described in CLSI document M27-A3 was employed for *in vitro* antifungal susceptibility testing (52). The stock solutions of allicin (50 mg mL^{-1}) and AmB (3.2 mg mL^{-1}) were prepared in dimethyl sulfoxide (DMSO; Sigma, USA), while FCZ (1.28 mg mL^{-1}) was dissolved in sterile distilled water. The stock solutions were then diluted with RPMI 1640 medium to prepare the working solution. The highest final concentrations used in 96-well polystyrene plates were $256\text{ }\mu\text{g mL}^{-1}$ for allicin (MCE, Shanghai, China), $128\text{ }\mu\text{g mL}^{-1}$ for FCZ (Sigma, USA), and $16\text{ }\mu\text{g mL}^{-1}$ for AmB (Sigma-Aldrich, USA). The MICs were determined as the lowest drug concentrations required to inhibit visible *T. asahii* growth. After 48 h of incubation, MIC_{50s} of FCZ and MIC_{100s} of AmB were determined. The MIC_{50s} and MIC_{90s} of allicin against *T. asahii* were determined after 24 and 48 h of incubation, respectively.

Determination of MFCs. The MFCs were determined by the method reported by Cantón et al. (53). Briefly, a $100\text{-}\mu\text{L}$ suspension from each MIC well was spread onto PDA plates and incubated at 35°C for 48 h. The MFC was defined as the minimum concentration that killed 99.9% of the inocula.

Spot assay. Overnight cultures of *T. asahii* in yeast-extract peptone dextrose (YPD) medium were collected, washed, and resuspended in saline solution ($1 \times 10^7\text{ CFU mL}^{-1}$). Serial 10-fold dilutions supplemented with allicin were transferred to 96-well plates and incubated for 8 h at 30°C and 300 rpm. Then, $20\text{-}\mu\text{L}$ aliquots of each well were spotted on PDA plates and cultured overnight at 35°C . The *T. asahii* colonies were photographed at the end of incubation.

Time-kill studies. Experiments were conducted as suggested by Cordeiro et al. with adaptations (54). The *T. asahii* yeast suspension ($5 \times 10^5\text{ CFU mL}^{-1}$) was incubated in RPMI 1640 medium (pH 7.0 with 0.165 M morpholinepropanesulfonic acid [MOPS]) supplemented with allicin ($0.5\times$, $1\times$, and $2\times$ MFC) at 35°C . At specified time points (0, 2, 4, 8, 24, and 48 h), 10-fold serial dilutions of suspension were streaked onto PDA plates, and the number of CFU was calculated after an additional 48 h of incubation at 35°C . The minimum detectable level was set at 100 CFU/mL . Growth controls were performed using RPMI medium without drugs. At least three independent experiments were conducted.

Biofilm assay. Overnight cultures of *T. asahii* grown in YPD medium were collected, washed, and resuspended in RPMI 1640 medium to $1 \times 10^6\text{ CFU mL}^{-1}$ for inoculation. Aliquots ($200\text{ }\mu\text{L}$ per well) of inoculum were then dispensed into flat 96-well polystyrene plates and incubated at 35°C . *T. asahii* cells adsorbed to the bottom of plates after 6 h of incubation, marking the adhesion stage of biofilms. The cells were then washed gently with sterile phosphate-buffered saline (PBS) before an additional 24 h and 48 h of incubation, representing the development and maturation stages of biofilms, respectively. Allicin was administered to biofilms cells at various stages, with the highest final concentrations of $256\text{ }\mu\text{g mL}^{-1}$ for biofilms cells in the adhesion stage and $512\text{ }\mu\text{g mL}^{-1}$ for those in the development and maturation stages. Metabolic activity and total biomass of *T. asahii* biofilms were evaluated using the XTT reduction assay (55) and the crystal violet assay (56), respectively. Untreated *T. asahii* biofilm cells served as the control. Biofilm assays were conducted in triplicate.

Cell surface hydrophobicity assay. The CSH experiment was performed using a water-hydrocarbon two-phase assay, as described by Kurakado et al. with adaptations (29). Briefly, *T. asahii* strains were cultured in YPD medium at 35°C overnight. Overnight cultures were transplanted into RPMI 1640 medium supplemented with allicin and incubated for 8 h at 30°C with shaking at 120 rpm. Subsequently, *T. asahii* cells were collected, washed, and resuspended in sterile PBS to an A_{600} of 1.0. Then, 1.2-mL aliquots of suspension were mixed with 0.3 mL octane (Damao, Tianjin, China) and incubated for 15 min incubation at 37°C in a water bath. The mixture was then vortexed for 5 min and allowed to stand until two phases separated. The absorbances of the aqueous phase were measured at 630 nm , with aliquots without octane overlay serving as the control. The relative cell surface hydrophobicity was calculated as follows: $[(A_{630}\text{ of the control} - A_{630}\text{ of octane overlay})/A_{630}\text{ of the control}] \times 100$. Experiments were performed in triplicate.

ROS assay. The ROS level was assessed as described by Lei et al. (57). *T. asahii* suspensions ($5 \times 10^5\text{ CFU mL}^{-1}$) in RPMI 1640 medium were plated in 24-well plates and incubated for 6 h at 35°C ,

followed by exposure to allicin for 6 h at 30°C. *T. asahii* cells were then stained with 10 $\mu\text{mol L}^{-1}$ DCFH-DA (Goyoo, China) for 20 min at 35°C. After that, *T. asahii* cells were washed with sterile PBS to remove remaining DCFH-DA and then observed under a fluorescence microscope at 488 nm. Untreated cells served as the control.

Ergosterol assay and sorbitol assay. The ergosterol and sorbitol assays were performed according to the procedure described by Turecka et al. with adaptations (58). For ergosterol assays, ergosterol (Psaitong, China) was first dissolved in trichloromethane and then diluted with RPMI 1640 medium. The MICs of allicin against *T. asahii* were determined using the broth microdilution method, as previously described, in the presence or absence of exogenous ergosterol. The ergosterol concentration in 96-well plates was finally adjusted to 200 $\mu\text{g mL}^{-1}$, with AmB serving as the positive control. For sorbitol assays, sorbitol (Psaitong, China) was dissolved directly in RPMI 1640 medium and filtered through 0.22- μm filters after being adjusted to a concentration of 1.6 M. The MICs of allicin against *T. asahii* were determined in the presence or absence of sorbitol with a final concentration of 0.8 M. AmB was used as a negative control. In both studies, the MICs were evaluated at 48 h. Each treatment was carried out in triplicate.

SEM. The overnight cultures of *T. asahii* in YPD medium were collected and adjusted to 1×10^7 CFU mL^{-1} in sterile saline solution. Subsequently, the *T. asahii* cell suspension was treated with allicin ($0\times$ or $1\times$ MFC) and incubated for 12 h at 30°C. Following fixation and dehydration procedures outlined by Lan et al. (59), cell images were captured using a TM3000 SEM (Hitachi, Japan).

TEM. The allicin treatment used for SEM analysis was also employed for TEM analysis of *T. asahii* cells, with fixation and dehydration procedures described by Turecka et al. (58). The ultrastructure of *T. asahii* cells was observed using a CM100 TEM (Philips, Netherlands).

CLSM. CLSM analysis was used to assess the effects of allicin on the structure and viability of biofilms. *T. asahii* cells were cultured in RPMI 1640 medium at 35°C for 6 h in 24-well polystyrene plates, resulting in the adhesion stage of biofilms. The plates were then washed with sterile PBS before biofilm cells were treated by allicin for 24 h at 30°C. After that, the biofilms were stained with a LIVE/DEAD BacLight bacterial viability kit (Thermo Fisher Scientific, USA) for 20 min at 35°C. Viable cells stained with SYTO 9 were observed at 485 nm using a TCS-SP8 CLSM (Leica, Germany), while dead and damaged cells stained with propidium iodide (PI) were observed at 535 nm.

Murine systemic trichosporonosis model. Male 6- to 8-week-old ICR mice (20 to 22 g) were obtained from SPF Biotechnology (Beijing, China) and housed in standard cages with *ad libitum* access to water and food. Mice were kept at 21 to 23°C under an appropriate light period. Before the experiments, mice were fed for 1 week to allow them to adapt to the new environment. Animal experiments were approved by the animal ethics committee of the Seventh Medical Center of PLA General Hospital, with ethics number no. 145 in 2022.

Prior to *T. asahii* inoculation, mice were first immunosuppressed for 3 days with a single intraperitoneal (i.p.) injection of cyclophosphamide (Endoxan, Germany) at a dose of 200 mg kg^{-1} per day. The yeast suspension of *T. asahii* BMT 06-3-09 was then prepared and adjusted in physiological saline to 10^7 CFU mL^{-1} . In order to induce systemic infection, yeast suspension was injected into the lateral tail vein at a dose of 0.2 mL per mouse. Mice were randomly divided into three groups ($n = 15$). The experimental groups received allicin via lateral tail vein injection at doses of either 10 mg kg^{-1} or 20 mg kg^{-1} , while the control groups received an equivalent volume of physiological saline (0.2 mL per mouse). For survival analysis, 10 mice were allocated to each group and monitored daily until day 14 postinoculation. Tissue fungal burden analysis was conducted using five mice per group, which were sacrificed at 5 days postinoculation. Spleens, kidneys, and livers were aseptically removed, weighed, and homogenized in 1 mL sterile saline. Serial 10-fold dilutions of the homogenates were plated on PDA and incubated for 48 h at 35°C. The numbers of CFU per gram of tissue were then calculated. Organs were embedded, sectioned, and stained with Gomori's methenamine silver (GMS) staining kit for histopathological examination.

RNA-Seq. The initial inoculum of the *T. asahii* CBS 2479 cells were adjusted to a 0.5 McFarland standard in 20 mL YPD medium and cultured for 12 h at 35°C with shaking at 120 rpm. The treated group was then exposed to allicin at a final concentration of 256 $\mu\text{g mL}^{-1}$. The cells were collected and washed three times with sterile PBS after 8 h treatment at 30°C. The samples were then quickly frozen in liquid nitrogen and stored at -80°C until required. The untreated *T. asahii* cells served as the control. Three independent cultures were used for RNA-Seq analysis. The transcriptome experiment was performed by Gene Denovo Biotechnology Co. (Guangzhou, China) with the following steps: total RNA extraction, mRNA enrichment by oligo(dT), RNA fragmentation, random-hexamer-primed cDNA synthesis, size selection, PCR amplification, and sequencing on an Illumina HiSeq 2500 (60).

The paired-end clean reads were aligned to the *T. asahii* strain CBS 2479 reference genome (<https://www.ncbi.nlm.nih.gov/genome/?term=CBS+2479>) using HISAT2.2.4. An FPKM (fragments per kilobase of transcript per million mapped reads) value was calculated to normalize gene expression for comparing samples. The DESeq2 software was used to identify DEGs between allicin-exposed and control groups based on an FDR of less than 0.05 and an absolute FC of ≥ 1.5 .

To investigate the biological functions of DEGs, GO (<http://geneontology.org/>) enrichment analysis and KEGG (<https://www.genome.jp/kegg/>) pathway enrichment analysis were performed. PHI-base (<http://www.phi-base.org/>) analysis was performed to explore the phenotypes involved in pathogenicity and virulence among the DEGs.

qRT-PCR analysis. To verify the results of RNA-Seq, five genes were randomly selected to confirm their expression by qRT-PCR analysis. The cDNA was synthesized by reverse transcription using the HiScript II Q RT SuperMix for qPCR (+gDNA wiper) kit (Vazyme, Nanjing, China). The sequences of primers are listed in Table S7. PCR was then performed using the ChamQ SYBR qPCR master mix (high ROX premixed) kit (Vazyme, Nanjing, China) and a TL988 real-time PCR system (Tianlong, Xian, China). The

reaction was conducted under the following conditions: 95°C for 90 s, followed by a total of 40 cycles of denaturation at 95°C for 5 s, annealing at 60°C for 15 s, and extension at 72°C for 20 s. The relative quantification of gene expression was computed using the $2^{-\Delta\Delta CT}$ method and 18S rRNA as an internal reference. For qRT-PCR experiments, three biological replicates were carried out.

Statistical analysis. Statistical analyses were carried out using the GraphPad Prism 8.3.0 (GraphPad Software, San Diego, CA, USA) and the results were expressed as means and standard deviations (SD). Survival data were assessed by the Kaplan-Meier curve with the log-rank chi square test. Statistical differences between multiple groups were compared using one-way analysis of variance (ANOVA) followed by Tukey's posttest. Statistical significance was set at probability (*P*) values of less than 0.05, 0.01, or 0.001.

Data availability. The data sets presented in this study have been deposited in the National Genomics Data Center (NGDC: <https://ngdc.cncb.ac.cn/>) and are accessible through GSA accession number CRA009653.

SUPPLEMENTAL MATERIAL

Supplemental material is available online only.

SUPPLEMENTAL FILE 1, PDF file, 0.3 MB.

SUPPLEMENTAL FILE 2, XLS file, 1.1 MB.

ACKNOWLEDGMENTS

We are grateful to Guangzhou Gene Denovo Biotechnology Co., Ltd., for assisting in sequencing.

X.Y. executed the experiments and original draft writing. S.B., J.W., Y.F., Z.X., and J.A. performed experiments. Y.Z. and T.C. collected and analyzed data. M.Z. and R.Y. conceived and led the research. All authors read, edited, and approved the submitted version.

This study was financially supported by the National Natural Science Foundation of China (no. 82073466, 82002120, and 81471928), Beijing Natural Science Foundation, China (no. 7212105 and 7202201), and the National Science Foundation of Chongqing, China (no. cstc2021jcyj-msxmX0140).

We declare no conflicts of interest.

REFERENCES

- Casalini G, Giacomelli A, Ridolfo A, Gervasoni C, Antinori S. 2021. Invasive fungal infections complicating COVID-19: a narrative review. *J Fungi* 7: 921. <https://doi.org/10.3390/jof7110921>.
- Ali GA, Husain A, Salah H, Goravey W. 2021. Trichosporon asahii fungemia and COVID-19 co-infection: an emerging fungal pathogen; case report and review of the literature. *IDCases* 25:e01244. <https://doi.org/10.1016/j.idcr.2021.e01244>.
- Sprute R, Cornely OA, Chen SC, Seidel D, Schuetz AN, Zhang SX. 2021. All you need to know and more about the diagnosis and management of rare yeast infections. *mBio* 12:e01594-21. <https://doi.org/10.1128/mBio.01594-21>.
- Benelli JL, Basso RP, Grafulha TW, Poester VR, Munhoz LS, Martins KB, Zogbi HE, Von Groll A, Severo CB, Stevens DA, Xavier MO. 2022. Fungal bloodstream co-infection by Trichosporon asahii in a COVID-19 critical patient: case report and literature review. *Mycopathologia* 187:397–404. <https://doi.org/10.1007/s11046-022-00637-6>.
- Colombo AL, Padovan AC, Chaves GM. 2011. Current knowledge of Trichosporon spp. and Trichosporonosis. *Clin Microbiol Rev* 24:682–700. <https://doi.org/10.1128/CMR.00003-11>.
- Sprute R, Bethe U, Chen SC, Cornely OA. 2022. EQUAL Trichosporon Score 2022: an ECMM score to measure QUALity of the clinical management of invasive Trichosporon infections. *J Antimicrob Chemother* 77:1779–1784. <https://doi.org/10.1093/jac/dkac085>.
- Liao Y, Lu X, Yang S, Luo Y, Chen Q, Yang R. 2015. Epidemiology and outcome of trichosporon fungemia: a review of 185 reported cases from 1975 to 2014. *Open Forum Infect Dis* 2:ofv141. <https://doi.org/10.1093/ofid/ofv141>.
- Wolf DG, Falk R, Hacham M, Theelen B, Boekhout T, Scorzetti G, Shapiro M, Block C, Salkin IF, Polachek I. 2001. Multidrug-resistant Trichosporon asahii infection of nongranulocytopenic patients in three intensive care units. *J Clin Microbiol* 39:4420–4425. <https://doi.org/10.1128/JCM.39.12.4420-4425.2001>.
- Oliveira dos Santos C, Zijlstra JG, Porte RJ, Kampinga GA, van Diepeningen AD, Sinha B, Bathoorn E. 2016. Emerging pan-resistance in Trichosporon species: a case report. *BMC Infect Dis* 16:148. <https://doi.org/10.1186/s12879-016-1477-3>.
- Adegboye O, Field MA, Kupz A, Pai S, Sharma D, Smout MJ, Wangchuk P, Wong Y, Loiseau C. 2021. Natural-product-based solutions for tropical infectious diseases. *Clin Microbiol Rev* 34:e00348-20. <https://doi.org/10.1128/CMR.00348-20>.
- Pancu DF, Scurtu A, Macasoi IG, Marti D, Mioc M, Soica C, Coricovac D, Horhat D, Poenaru M, Dehelean C. 2021. Antibiotics: conventional therapy and natural compounds with antibacterial activity—a pharmaco-toxicological screening. *Antibiotics (Basel)* 10:401. <https://doi.org/10.3390/antibiotics10040401>.
- Salehi B, Zucca P, Orhan IE, Azzini E, Adetunji CO, Mohammed SA, Banerjee SK, Sharopov F, Rigano D, Sharifi-Rad J, Armstrong L, Martorell M, Sureda A, Martins N, Selamoğlu Z, Ahmad Z. 2019. Allicin and health: a comprehensive review. *Trends Food Sci Technol* 86:502–516. <https://doi.org/10.1016/j.tifs.2019.03.003>.
- Marchese A, Barbieri R, Sanches-Silva A, Daglia M, Nabavi SF, Jafari NJ, Izadi M, Ajami M, Nabavi SM. 2016. Antifungal and antibacterial activities of allicin: a review. *Trends Food Sci Technol* 52:49–56. <https://doi.org/10.1016/j.tifs.2016.03.010>.
- Felli Kubica T, Bedin Denardi L, Silva de Loreto E, Zeni G, Weiblen C, Oliveira V, Morais Santurio J, Hartz Alves S. 2019. In vitro activity of diphenyl diselenide and ebselen alone and in combination with antifungal agents against Trichosporon asahii. *Mycoses* 62:428–433. <https://doi.org/10.1111/myc.12906>.
- Torrado JJ, Espada R, Ballesteros MP, Torrado-Santiago S. 2008. Amphotericin B formulations and drug targeting. *J Pharm Sci* 97:2405–2425. <https://doi.org/10.1002/jps.21179>.
- Montanes FM, Pascual-Ahuir A, Proft M. 2011. Repression of ergosterol biosynthesis is essential for stress resistance and is mediated by the Hog1 MAP kinase and the Mot3 and Rox1 transcription factors. *Mol Microbiol* 79:1008–1023. <https://doi.org/10.1111/j.1365-2958.2010.07502.x>.
- Robbins N, Wright GD, Cowen LE. 2016. Antifungal drugs: the current armamentarium and development of new agents. *Microbiol Spectr* 4:FUNK-0002-2016. <https://doi.org/10.1128/microbiolspec.FUNK-0002-2016>.
- El-Saber Batiha G, Magdy Beshbishy A, L GW, Elewa YHA, A AA-S, Abd El-Hack ME, Taha AE, Y MA-E, Prasad Devkota H. 2020. Chemical constituents and pharmacological activities of garlic (*Allium sativum* L.): a review. *Nutrients* 12:872. <https://doi.org/10.3390/nu12030872>.

19. Borlinghaus J, Foerster Nee Reiter J, Kappler U, Antelmann H, Noll U, Gruhlke MCH, Sularesenko AJ. 2021. Allicin, the odor of freshly crushed garlic: a review of recent progress in understanding allicin's effects on cells. *Molecules* 26:1505. <https://doi.org/10.3390/molecules26061505>.
20. An M, Shen H, Cao Y, Zhang J, Cai Y, Wang R, Jiang Y. 2009. Allicin enhances the oxidative damage effect of amphotericin B against *Candida albicans*. *Int J Antimicrob Agents* 33:258–263. <https://doi.org/10.1016/j.ijantimicag.2008.09.014>.
21. Zhou YB, Xiao YY, Chao JJ, Ma L. 2021. In vitro activity of allicin alone and in combination with antifungal drugs against *Microsporum canis* isolated from patients with tinea capitis. *Front Med (Lausanne)* 8:783086. <https://doi.org/10.3389/fmed.2021.783086>.
22. Jia Y, Wu X. 2017. In vitro activity of allicin combined with two antibiotics on intestinal *Shigella*. *Infect Int* 6:25–29. <https://doi.org/10.1515/ii-2017-0152>.
23. Kim J, Kim MJ, Chong YP, Kim SH, Choi SH, Lee SO, Woo JH, Kim YS, Jung J. 2021. Comparison of the characteristics of patients with invasive infections and noninvasive infections caused by *Trichosporon asahii*. *Med Mycol* 59:296–300. <https://doi.org/10.1093/mmy/myaa076>.
24. Zainal M, Mohamad Zain N, Mohd Amin I, Ahmad VN. 2021. The antimicrobial and antibiofilm properties of allicin against *Candida albicans* and *Staphylococcus aureus* - a therapeutic potential for denture stomatitis. *Saudi Dent J* 33:105–111. <https://doi.org/10.1016/j.sdentj.2020.01.008>.
25. Yang X, Sha K, Xu G, Tian H, Wang X, Chen S, Wang Y, Li J, Chen J, Huang N. 2016. Subinhibitory concentrations of allicin decrease uropathogenic *Escherichia coli* (UPEC) biofilm formation, adhesion ability, and swimming motility. *Int J Mol Sci* 17:979. <https://doi.org/10.3390/ijms17070979>.
26. Ranjbar-Omid M, Arzanlou M, Amani M, Shokri Al-Hashem SK, Amir Mozafari N, Peeri Doghaheh H. 2015. Allicin from garlic inhibits the biofilm formation and urease activity of *Proteus mirabilis* in vitro. *FEMS Microbiol Lett* 362:fnv049. <https://doi.org/10.1093/femsle/fnv049>.
27. Khodavandi A, Harmal NS, Alizadeh F, Scully OJ, Sidik SM, Othman F, Sekawi Z, Ng KP, Chong PP. 2011. Comparison between allicin and fluconazole in *Candida albicans* biofilm inhibition and in suppression of HWP1 gene expression. *Phytomedicine* 19:56–63. <https://doi.org/10.1016/j.phymed.2011.08.060>.
28. Nobile CJ, Nett JE, Andes DR, Mitchell AP. 2006. Function of *Candida albicans* adhesin Hwp1 in biofilm formation. *Eukaryot Cell* 5:1604–1610. <https://doi.org/10.1128/EC.00194-06>.
29. Kurakado S, Miyashita T, Chiba R, Sato C, Matsumoto Y, Sugita T. 2021. Role of arthroconidia in biofilm formation by *Trichosporon asahii*. *Mycoses* 64:42–47. <https://doi.org/10.1111/myc.13181>.
30. Di Bonaventura G, Pompilio A, Piccini C, Iezzi M, D'Antonio D, Piccolomini R. 2006. Biofilm formation by the emerging fungal pathogen *Trichosporon asahii*: development, architecture, and antifungal resistance. *Antimicrob Agents Chemother* 50:3269–3276. <https://doi.org/10.1128/AAC.00556-06>.
31. Koch HP, Lawson LD. 1996. Garlic: the science and therapeutic application of *Allium sativum* L. and related species. Williams & Wilkins, Baltimore, MD.
32. Ogita A, Fujita K, Tanaka T. 2009. Enhancement of the fungicidal activity of amphotericin B by allicin: effects on intracellular ergosterol trafficking. *Planta Med* 75:222–226. <https://doi.org/10.1055/s-0028-1088376>.
33. Li Z, Li Z, Yang J, Lu C, Li Y, Luo Y, Cong F, Shi R, Wang Z, Chen H, Li X, Yang J, Ye F. 2022. Allicin shows antifungal efficacy against *Cryptococcus neoformans* by blocking the fungal cell membrane. *Front Microbiol* 13:1012516. <https://doi.org/10.3389/fmicb.2022.1012516>.
34. Aala F, Yusuf UK, Nulit R, Rezaie S. 2014. Inhibitory effect of allicin and garlic extracts on growth of cultured hyphae. *Iran J Basic Med Sci* 17:150–154.
35. Kim YS, Kim KS, Han I, Kim MH, Jung MH, Park HK. 2012. Quantitative and qualitative analysis of the antifungal activity of allicin alone and in combination with antifungal drugs. *PLoS One* 7:e38242. <https://doi.org/10.1371/journal.pone.0038242>.
36. Getti GTM, Poole PL. 2019. Allicin causes fragmentation of the peptidoglycan coat in *Staphylococcus aureus* by effecting synthesis and aiding hydrolysis: a determination by MALDI-TOF mass spectrometry on whole cells. *J Med Microbiol* 68:667–677. <https://doi.org/10.1099/jmm.0.000950>.
37. Choo S, Chong PP, Tay ST, Wong EH, Madhavan P, Yong P. 2020. Inhibition of sessile and biofilm growth in various *Aspergillus* species by allicin associated with disruption to structural changes in cell wall. *Int J Infect Dis* 101:71. <https://doi.org/10.1016/j.ijid.2020.09.215>.
38. Sajali N, Mohd Desa MN, Than LTL, Chin VK, Chong PP. 2020. Allicin modulates expression of cell wall-related genes in *Aspergillus fumigatus*. *Int J Infect Dis* 101:394. <https://doi.org/10.1016/j.ijid.2020.09.1033>.
39. Samalova M, Carr P, Bromley M, Blatzer M, Moya-Nilges M, Latge JP, Mouyna I. 2020. GPI anchored proteins in *Aspergillus fumigatus* and cell wall morphogenesis. *Curr Top Microbiol Immunol* 425:167–186. https://doi.org/10.1007/82_2020_207.
40. Lozancic M, Zunar B, Hrestak D, Lopandic K, Teparic R, Mrsa V. 2021. Systematic comparison of cell wall-related proteins of different yeasts. *J Fungi* 7:128. <https://doi.org/10.3390/jof7020128>.
41. Lima SL, Colombo AL, de Almeida Junior JN. 2019. Fungal cell wall: emerging antifungals and drug resistance. *Front Microbiol* 10:2573. <https://doi.org/10.3389/fmicb.2019.02573>.
42. Rich PR, Marechal A. 2010. The mitochondrial respiratory chain. *Essays Biochem* 47:1–23. <https://doi.org/10.1042/bse0470001>.
43. Fernie AR, Carrari F, Sweetlove LJ. 2004. Respiratory metabolism: glycolysis, the TCA cycle and mitochondrial electron transport. *Curr Opin Plant Biol* 7:254–261. <https://doi.org/10.1016/j.pbi.2004.03.007>.
44. Nolfi-Donagan D, Braganza A, Shiva S. 2020. Mitochondrial electron transport chain: oxidative phosphorylation, oxidant production, and methods of measurement. *Redox Biol* 37:101674. <https://doi.org/10.1016/j.redox.2020.101674>.
45. Ha KP, Clarke RS, Kim GL, Brittan JL, Rowley JE, Mavridou DAI, Parker D, Clarke TB, Nobbs AH, Edwards AM. 2020. Staphylococcal DNA repair is required for infection. *mBio* 11:e02288-20. <https://doi.org/10.1128/mBio.02288-20>.
46. Zhang B, Pan C, Feng C, Yan C, Yu Y, Chen Z, Guo C, Wang X. 2022. Role of mitochondrial reactive oxygen species in homeostasis regulation. *Redox Rep* 27:45–52. <https://doi.org/10.1080/13510002.2022.2046423>.
47. Staerck C, Gastebois A, Vandeputte P, Calenda A, Larcher G, Gillmann L, Papon N, Bouchara JP, Fleury MJJ. 2017. Microbial antioxidant defense enzymes. *Microb Pathog* 110:56–65. <https://doi.org/10.1016/j.micpath.2017.06.015>.
48. Viglas J, Olejnikova P. 2021. An update on ABC transporters of filamentous fungi - from physiological substrates to xenobiotics. *Microbiol Res* 246:126684. <https://doi.org/10.1016/j.micres.2020.126684>.
49. Urban M, Cuzick A, Seager J, Wood V, Rutherford K, Venkatesh SY, De Silva N, Martinez MC, Pedro H, Yates AD, Hassani-Pak K, Hammond-Kosack KE. 2020. PHI-base: the pathogen-host interactions database. *Nucleic Acids Res* 48:D613–D620. <https://doi.org/10.1093/nar/gkz904>.
50. Choo S, Chin VK, Wong EH, Madhavan P, Tay ST, Yong PVC, Chong PP. 2020. Review: antimicrobial properties of allicin used alone or in combination with other medications. *Folia Microbiol (Praha)* 65:451–465. <https://doi.org/10.1007/s12223-020-00786-5>.
51. Kubica TF, Denardi LB, Azevedo MI, Oliveira V, Severo LC, Santurio JM, Alves SH. 2016. Antifungal activities of tacrolimus in combination with antifungal agents against fluconazole-susceptible and fluconazole-resistant *Trichosporon asahii* isolates. *Braz J Infect Dis* 20:539–545. <https://doi.org/10.1016/j.bjid.2016.08.008>.
52. Clinical and Laboratory Standards Institute. 2008. Reference method for broth dilution antifungal susceptibility testing of yeasts. Approved standard, 3rd ed. CLSI document M27-A3. Clinical and Laboratory Standards Institute, Wayne, PA.
53. Canton E, Peman J, Valentin A, Bosch M, Espinel-Ingroff A, Gobernado M. 2008. Comparison of posaconazole and voriconazole in vitro killing against *Candida krusei*. *Diagn Microbiol Infect Dis* 62:177–181. <https://doi.org/10.1016/j.diagmicrobio.2008.07.001>.
54. Cordeiro RA, Wesley Caracés Cedro E, Raquel Colares Andrade A, Serpa R, Jose de Jesus Evangelista A, Sales de Oliveira J, Santos Pereira V, Pereira Alencar L, Bruna Leite Mendes P, Cibelle Soares Farias B, Maria Maciel Melo V, Pires de Camargo Z, de Souza Collares Maia Castelo-Branco D, Samia Nogueira Brilhante R, Julio Costa Sidrim J, Fabio Gadelha Rocha M. 2018. Inhibitory effect of a lipopeptide biosurfactant produced by *Bacillus subtilis* on planktonic and sessile cells of *Trichosporon* spp. *Biofouling* 34:309–319. <https://doi.org/10.1080/08927014.2018.1437617>.
55. de Aguiar Cordeiro R, Serpa R, Flavia Uchoa Alexandre C, de Farias Marques FJ, Vladia Silva de Melo C, da Silva Franco J, Jose de Jesus Evangelista A, Pires de Camargo Z, Samia Nogueira Brilhante R, Fabio Gadelha Rocha M, Luciano Bezerra Moreira J, de Jesus Pinheiro Gomes Bandeira T, Julio Costa Sidrim J. 2015. *Trichosporon* inkin biofilms produce extracellular proteases and exhibit resistance to antifungals. *J Med Microbiol* 64:1277–1286. <https://doi.org/10.1099/jmm.0.000159>.
56. Iturrieta-Gonzalez IA, Padovan AC, Bizerra FC, Hahn RC, Colombo AL. 2014. Multiple species of *Trichosporon* produce biofilms highly resistant to triazoles and amphotericin B. *PLoS One* 9:e109553. <https://doi.org/10.1371/journal.pone.0109553>.
57. Lei S, Zhao H, Pang B, Qu R, Lian Z, Jiang C, Shao D, Huang Q, Jin M, Shi J. 2019. Capability of iturin from *Bacillus subtilis* to inhibit *Candida albicans*

- in vitro and in vivo. *Appl Microbiol Biotechnol* 103:4377–4392. <https://doi.org/10.1007/s00253-019-09805-z>.
58. Turecka K, Chylewska A, Kawiak A, Waleron KF. 2018. Antifungal activity and mechanism of action of the Co(III) coordination complexes with diamine chelate ligands against reference and clinical strains of *Candida* spp. *Front Microbiol* 9:1594. <https://doi.org/10.3389/fmicb.2018.01594>.
59. Lan Y, Lu S, Zheng B, Tang Z, Li J, Zhang J. 2021. Combinatory effect of ALA-PDT and itraconazole treatment for *Trichosporon asahii*. *Lasers Surg Med* 53:722–730. <https://doi.org/10.1002/lsm.23343>.
60. Li L, Pan H, Deng L, Qian G, Wang Z, Li W, Zhong C. 2022. The antifungal activity and mechanism of silver nanoparticles against four pathogens causing kiwifruit post-harvest rot. *Front Microbiol* 13:988633. <https://doi.org/10.3389/fmicb.2022.988633>.